Published in final edited form as:
Invest Ophthalmol Vis Sci. 2010 April ; 51(4): 2149–2157. doi:10.1167/iovs.09-3817.

Imaging of the Retinal Pigment Epithelium in Age-Related Macular Degeneration Using Polarization-Sensitive Optical Coherence Tomography

Christian Ahlers[1], **Erich Götzinger**[2], **Michael Pircher**[2], **Isabelle Golbaz**[1], **Franz Prager**[1], **Christopher Schütze**[1], **Bernhard Baumann**[2], **Christoph K. Hitzenberger**[2], and **Ursula Schmidt-Erfurth**[1]

[1]Department of Ophthalmology, Medical University of Vienna, Vienna, Austria

[2]Center for Biomedical Engineering and Physics, Medical University of Vienna, Vienna, Austria

Abstract

Purpose—Spectral-domain optical coherence tomography (SD-OCT) provides new insights into the understanding of age-related macular degeneration (AMD) but limited information on the nature of hyperreflective tissue at the level of the retinal pigment epithelium. Therefore, polarization-sensitive (PS) SD-OCT was used to identify and characterize typical RPE findings in AMD.

Methods—Forty-four eyes of 44 patients with AMD were included in this prospective case series representing the entire AMD spectrum from drusen ($n = 11$), geographic atrophy (GA; $n = 11$), neovascular AMD (nAMD; $n = 11$) to fibrotic scars ($n = 11$). Imaging systems were used for comparative imaging. A PS-SD-OCT instrument was developed that was capable of recording intensity and polarization parameters simultaneously during a single scan.

Results—In drusen, PS-SD-OCT identified a continuous RPE layer with focal elevations. Discrete RPE atrophy (RA) could be observed in two patients. In GA, the extension of the RA was significantly larger. Residual RPE islands could be detected within the atrophic zone. PS-SD-OCT identified multiple foci of RPE loss in patients with nAMD and allowed recognition of advanced RPE disease associated with choroidal neovascularization. Wide areas of RA containing residual spots of intact retinal pigment epithelium could be identified in fibrotic scars.

Conclusions—PS-SD-OCT provided precise identification of retinal pigment epithelium in AMD. Recognition of these disease-specific RA patterns in dry and wet forms of AMD is of particular relevance to identify the status and progression of RPE disease and may help to better estimate the functional prognosis of AMD.

Age-related macular degeneration (AMD) is the leading cause of blindness in persons aged 60 and older in the developed world.[1] The number of patients is steadily increasing and is expected to double by the year 2020, causing distinct challenges for health care systems.[2–5] Although these facts are alarming, only 1 in 10 patients has the neovascular form of AMD

Corresponding author: Ursula Schmidt-Erfurth, Department of Ophthalmology, Medical University of Vienna, Waehringer Guertel 18-20, Vienna, Austria; ursula.schmidt-erfurth@meduniwien.ac.at..

Disclosure: **C. Ahlers**, None; **E. Götzinger**, None; **M. Pircher**, None; **I. Golbaz**, None; **F. Prager**, None; **C. Schütze**, None; **B. Baumann**, None; **C.K. Hitzenberger**, None; **U. Schmidt-Erfurth**, None

Presented at the annual meeting of the Association for Research in Vision and Ophthalmology, Fort Lauderdale, Florida, May 2008, and at the annual meeting of the German Society of Ophthalmology, Berlin, Germany, September 2008.

Europe PMC Funders Author Manuscripts

(nAMD) for which therapeutic methods, such as the inhibition of vascular endothelial growth factor (VEGF), have been developed in recent years.[6,7]

Dry forms of AMD (dAMD), clinically appearing as drusen (DN) or geographic atrophy (GA), affect most patients with AMD. It is recommended that these patients supplement their diets with vitamins, in accordance with AREDS guidelines, to reduce the risk for severe vision loss from atrophic or neovascular complications.[8] Upcoming treatment options for dAMD could therefore be used to treat high numbers of patients if the treatments can be proven effective.

Appropriate and objective technologies allowing insight into individualized prognosis and risk for complications are necessary to allocate the limited resources in an ethical, effective, and evidence-based manner. Optical coherence tomography (OCT) is expected to be one of these modalities because it facilitates time-efficient, noninvasive retinal imaging.[9-12] Even though higher resolution and enhanced imaging speed of current spectral domain (SD) OCT devices has clearly increased the value of OCT for the clinician, a limitation of OCT known from the time domain era has not yet been overcome. Recent studies indicate that improvements in morphometric parameters, such as retinal thickness and sub-RPE values, do not necessarily correlate with better visual function, especially after the initial treatment phase of antiangiogenic therapy in nAMD.[13-15] This finding is supported by the clinical impression that scarring or discrete GA might limit the visual prognosis in some patients under repeated anti-VEGF treatment.

Current SD-OCT technology, however, has distinct limitations, especially in displaying the integrity and status of the retinal pigment epithelium in AMD, because of difficulties in the correct segmentation and similar reflectivity of structures that do not represent functional retinal pigment epithelium in patients with nAMD. Moreover, it is unlikely that higher resolution or further advances in imaging speed will overcome this problem in the near future.

Because the retinal pigment epithelium is a most relevant structure in all forms of AMD, better understanding of a patient's underlying RPE status may facilitate an explanation of vision loss without a recurrence of intraretinal or subretinal fluid in nAMD under antiangiogenic therapy and a more accurate estimation of a patient's prognosis in both dAMD and nAMD.

Polarization-sensitive OCT (PS-OCT) is a novel technology that is capable of detecting the depolarizing properties of the retinal pigment epithelium in addition to gathering the information obtained by conventional SD-OCT scans.[16,17] In PS-OCT, information is gathered simultaneously during the same raster scan. PS-SD-OCT also enables[18] three-dimensional analysis. Very recently, we developed algorithms capable of segmenting the retinal pigment epithelium based on its depolarizing properties out of the datasets.[19] This procedure allows for true tissue differentiation between the retinal pigment epithelium and other hyperreflective structures on the basis of different intrinsic physical properties.

In addition to previous reports of our group,[20] we aimed in this study to investigate the three-dimensional integrity of the retinal pigment epithelium in patients with different forms and stages of AMD to identify the presence of RPE atrophy using the latest generation PS-SD-OCT device in combination with recently developed RPE segmentation algorithms.[19]

Patients and Methods

Inclusion Criteria and Patient Characteristics

Forty-four eyes of 44 consecutive Caucasian patients with drusen ($n = 11$), GA ($n = 11$), nAMD ($n = 11$), and fibrotic scars from nAMD ($n = 11$) were included. All patients underwent a standard ophthalmologic examination process. Fluorescence angiography was performed in all patients with nAMD.

Patients included in this study had to be older than 60 years of age. Previous vitreoretinal surgery or other concomitant ophthalmologic abnormalities were an exclusion criterion, as was aphakia. Written informed consent after a discussion of the perspectives and results was obtained from all patients before inclusion. The institutional ethics committee approved the procedures of the study including treatment and diagnostic examinations. The protocol complied with the standards of the Declaration of Helsinki. All examinations were performed at the Department of Ophthalmology and the Center for Biomedical Engineering and Physics, both at the Medical University Vienna in Austria.

Treatment of Patients Included in this Study

Patients with GA, drusen, or chorioretinal scars from nAMD were under strict ophthalmologic control (each fellow eye was included). These patients were treated with vitamin supplementation according to the AREDS guidelines, if appropriate. Patients with nAMD received intravitreal ranibizumab treatment on an SD-OCT-based treatment regimen. Retreatment criteria adhered to those suggested by the PRONTO study after a loading dose consisting of three monthly injections of ranibizumab was given.

Conventional SD-OCT Imaging

Patients were examined with various OCT systems (Stratus [Cirrus, Carl Zeiss Meditec], 3D-OCT-1000 [Topcon], and Spectralis [Heidelberg]). SD-OCT systems are capable of imaging the retina with high speed and high-resolution raster scans, enabling retinal thickness analysis and high-detail morphologic imaging. The Cirrus OCT and the Topcon OCT are able to display the contour of the estimated retinal pigment epithelium as a topographic map using the standard software.

PS-SD-OCT Imaging and RPE Segmentation Procedures

The PS-SD-OCT device used in this study is described elsewhere.[18] In brief, the system is capable of obtaining several parameters simultaneously: intensity (as in standard OCT imaging), retardation (phase shift introduced by birefringence between two orthogonal linear polarization states), fast axis orientation (birefringent axis orientation of the sample relative to the orientation of the instrument), and degree of polarization uniformity. The instrument is operated at an A-scan rate of 20,000 A-scans per second for each polarization channel, allowing the recording of 3D data sets covering a scan field of 15° × 15° and consisting of 1000 × 60 × 1024 pixels (x-y-z direction) in approximately 3 seconds. The total imaging depth was approximately 3 mm. The details of the segmentation algorithm used to identify the retinal pigment epithelium were recently published elsewhere.[19] Subsumed, the algorithm is based on the intrinsic tissue property of the retinal pigment epithelium that scrambles the polarization state of the backscattered light.[17] This polarization scrambling can be observed in a random variation of retardation (Fig. 1B, greenish band marked with an arrow) and axis orientation values from speckle to speckle. For a better description of this random variation, we calculated the elements of the Stokes vectors of the beam backscattered from the sample. With the elements of the Stokes vector, a degree of polarization (DOP) can be calculated. Note that because OCT is a coherent imaging technique, the DOP will always be 1 if calculated at each single data point. However, if we

average Stokes vectors over adjacent pixels by calculating the mean value of each Stokes vector element within a rectangular window (that is much larger than the speckle size), we can derive a quantity that we called the “degree of polarization uniformity” (DOPU). We used a floating window (size 15(x) × 6(z) pixels, or ~70(x) × 18(y) μm) for all calculations of the DOPU presented in this article (Fig. 1). Figure 1C shows an image containing DOPU information of a patient with drusen. The outline of the retinal pigment epithelium (green/blue band) is clearly visible and shows focal elevations of the drusen, as expected. To calculate retinal thickness maps, we used median filtering before the surface detection (edge detection) and defined the distance from the detected retinal surface to the segmented retinal pigment epithelium as retinal thickness. RPE elevation maps are generated by the arbitrary depth position of the segmented retinal pigment epithelium after subtraction of a mean position value (calculated by averaging all RPE positions in the y-direction). This procedure roughly removes influences from the relative position of the retina. To account for the anisotropic sampling of the generated images, all images were interpolated in the y-direction (by a factor of ~10).

Results

Early Dry AMD: Drusen

Drusen could be identified as local elevations of the retinal pigment epithelium in SD-OCT B scans. The current RPE segmentation algorithm provided by the Heidelberg OCT, however, often failed to identify these elevations correctly (Fig. 2). RPE deviation maps generated by Cirrus and Topcon clearly showed these elevations. Corresponding to these elevations caused by drusen, focal areas of retinal thinning could be observed in retinal thickness maps. Similar retinal thickness and RPE elevation maps could be generated from PS-SD-OCT data using the novel segmentation algorithm described in the methods section.

Moreover, small focal skip lesions (FSLs) could be detected within the depolarizing pattern of the retinal pigment epithelium in 2 of 11 patients. Figure 3 shows an exemplary B scan with clearly visible FSL (marked with circled in Fig. 3). These automatically detected skip lesions were confirmed by independent evaluation of OCT B-scans (intensity, retardation, and DOPU images) by three expert examiners to ensure that this observation was no artifact generated by the segmentation algorithm. Moreover, FSLs were counted only if they could be observed in at least two adjacent B-scan images. The reader may note that these FSLs within the retinal pigment epithelium could be detected only with PS-OCT because contrast based on intensity (standard OCT imaging) is very weak, and enhanced penetration depth from RPE atrophy is not always visible, especially in small lesions. In fact, a change within the retinal pigment epithelium might even be observed in the intensity image by an experienced observer if the location of the lesion is known before making use of information provided by PS-SD-OCT. However, these small changes in intensity could also be generated by other means (e.g., shadowing by blood vessels). Therefore, RPE maps generated using intensity images failed to identify these changes reliably and suggest a regular and continuous RPE appearance.

Advanced Dry AMD: Geographic Atrophy

GA appeared as focal retinal thinning over an atrophic zone of retinal pigment epithelium in histology and SD-OCT B-scan imaging. Enhanced penetration depth (visible as hyperreflective area below the RPE defect) could often be observed and typically extends down to the level of the sclera in B scans (Figs. 4A, 4D, 4G, 4J). Interestingly, the margin of the atrophic area often coincided with the location to which the signal of the external limiting membrane could be followed, down to the level of the RPE loss. Consistent with its pathophysiology, GA resulted in a circumscribed thinning in SD-OCT retinal thickness

analysis (Figs. 4B, 4E, 4M). However, significant differences could be visualized in SD-OCT retinal thickness maps. Diligent RPE analyses of RPE segmentation used in commercial systems showed that all algorithms failed to identify the RPE loss because the RPE segmentation inconsistently identified the Bruch's membrane/choriocapillaris complex as retinal pigment epithelium within the atrophic zone (Figs. 4A, 4D) and to simulate an irregular but continuous RPE layer (Fig. 4F). Maps of the retinal pigment epithelium consequently failed to detect the RPE atrophy showing inhomogeneous characteristics and no correlation to autofluorescence images. Consistently, retinal thickness maps varied between the different SD. OCT devices indicated that zones of retinal thinning did not necessarily correspond to the real atrophic zone. This effect is related to the segmentation algorithm, which is unable to distinguish between retinal pigment epithelium and Bruch's membrane on the basis of intensity-based data (Fig. 4E). To overcome this problem, the "slab" function integrated into the Cirrus software can be used to visualize the typical RPE transillumination present in GA (Figs. 4G, 4H; note the consistency between autofluorescence and transillumination in this patient).

In contrast, PS-SD-OCT was capable of precisely identifying the exact loss of depolarization in the affected regions in all patients. The segmentation algorithm provided reliable results even in the coexistent presence of irregularly shaped and partially elevated retinal pigment epithelium in the peri-marginal zones that surround the central gap in GA in most patients. Although the margins of the lesions are well defined in GA, an irregular appearance of depolarizing tissue could clearly be detected in the DOPU image at the lesions margins (Fig. 4L). Patterns of depolarizing signals in deeper layers could be segmented in all patients within extended zones of RPE atrophy (Fig. 4K). Figure 4M shows a conventional retinal thickness map obtained with PS-OCT (distances from either the retinal pigment epithelium or Bruch's membrane to the ILM are regarded as retinal thickness) for better comparison with other SD-OCT instruments. However, with PS-SD-OCT, an RPE thickness map (Fig. 4N) can be retrieved that clearly shows atrophic areas (displayed in light gray). Note the good correspondence of the PS-SD-OCT data with autofluorescence images (Fig. 4C) in this patient.

Neovascular AMD

Visual acuity was markedly reduced in patients with nAMD. Conventional SD-OCT enabled the differentiation of distinct retinal layers in the high-resolution B scans. Depending on lesion activity, SD-OCT examinations after antiangiogenic treatment frequently showed elevations and/or duplications of hyperreflective retinal structures (e.g., retinal pigment epithelium), with or without pigment epithelial detachment (PED), subretinal fluid, or intraretinal fluid. Retinal thickness maps provided by commercial instruments showed significant differences in retinal thickness measurements (Fig. 5). Moreover, conventional SD-OCT did often not allow us to judge which of the multiple hyperreflective layers actually represented the retinal pigment epithelium.

The Cirrus RPE map often shows an indentation at the margins of the PED (Fig. 5F), where subretinal fluid changes the architecture of the retinal layers and provokes an adjustment of the algorithm detecting the course of the retinal pigment epithelium. The Spectralis OCT often fails to detect the real RPE pattern in nAMD, whereas the segmentation process used in 3D-SD-OCT-1000 is often subject to inconsistent misdetections, especially of the posterior retinal surface (Figs. 5G, 5J). The different performance of the algorithms used by different manufacturers refers to the difficulties comparing retinal thickness measurements between different SD-OCT systems in nAMD.

RPE segmentation using PS-SD-OCT, however, is based on the intrinsic depolarizing tissue property of the retinal pigment epithelium. This approach allows detection of FSLs in the

irregular RPE pattern. B-scans of nAMD patients frequently showed an irregularly elevated, distorted, or thickened pattern with retinal pigment epithelium next to FSL. FSLs were generally larger than those observed in drusen. Foci of residual depolarization in deeper layers as observed in GA could not be seen in patients with nAMD (Fig. 6).

This finding may explain why visual acuity does not improve in some patients even though their retinal anatomy is quickly restored as a result of the consequent application of antiangiogenic treatment. Interestingly, most patients have FSLs at the margins of the lesion. Virtually all patients with FSLs have multiple FSLs. Peripheral RPE lesions (located outside the central 3 mm) were also present in most patients with nAMD in this study (Fig. 7).

End-Stage Neovascular Disease: Fibrotic Scars from nAMD

Large fibrotic scars from nAMD often signify the irreversible functional end point of neovascular AMD disease. SD-OCT typically showed severe intraretinal alterations accompanied by cysts and fluid in various retinal locations. Hyperreflective areas at the choriocapillary level from RPE atrophy, as observed in GA, could frequently be seen in PS-SD-OCT but usually appeared in a more irregular pattern. The retinal pigment epithelium could be observed as an indefinable thickened and hyperreflective tissue layer. Poor fixation often compromised the imaging process in SD- and PS-SD-OCT imaging.

In contrast to the intensity-based images, the DOPU image obtained with PS-SD-OCT detected small areas of residual depolarization within the scarred, hyperreflective tissue. Although the appearance of the atrophy was considerably different from the GA in this study, some similarities could be found. Small islands of depolarizing tissue that could be identified well below the level of the retinal pigment epithelium could frequently be observed in seven patients (Fig. 8). The histologic nature of these islands, however, remains uncertain.

Discussion

This study evaluated the status of the retinal pigment epithelium in different forms and stages of AMD progression using the novel PS-OCT technology compared with conventional, commercially available SD-OCT systems. In contrast to SD-OCT, PS-SD-OCT is capable of gathering additional information on the sample using the polarization properties of light. The PS-SD-OCT instrument enables several different physical quantities —intensity, retardation, birefringent axis orientation, and degree of polarization uniformity —to be obtained simultaneously within the same imaging process. The intrinsic tissue property of the retinal pigment epithelium to depolarize backscattered light can uniquely be used to identify the retinal pigment epithelium even in the presence of severe distortions of the physiologic retinal structure. New segmentation procedures[19] that use these RPE-specific tissue properties allowed us to investigate the segmented RPE layer of patients in all stages of AMD. Compared with the results of a recent study by Miura et al.,[21] who used laser imaging polarimetry to enhance image contrast in AMD patients, we were able to provide three-dimensional information of the retinal structure that included retinal thickness maps and retinal elevation maps in a wide spectrum of patients. Finally, we compared our results with measurements provided by current SD-OCT devices that are commercially available and present in many clinics. These comparisons showed some major limitations of conventional SD-OCT devices, which are unable to detect FSLs within the retinal pigment epithelium reliably in all forms of AMD. Even though signs of atrophy can though be observed in SD-OCT devices using image averaging, it must be taken into account that these systems do not provide the highest resolution images for a complete 3D data set.

RPE maps provided by conventional SD-OCT instruments might therefore be misleading in the clinical evaluation of AMD with localized RPE atrophy. Errors in the correct detection of the retinal pigment epithelium have been identified in previous studies[14,22] and are related to the limited tissue differentiation of all intensity-based OCT and SD-OCT devices. However, it must be remembered that RPE mapping procedures integrated in current SD-OCT devices were not primarily intended to outline RPE defects. It therefore remains unclear how specially adapted software solutions for these devices aimed to identify regions of RPE atrophy on the basis of abrupt reflectivity changes in the retinal pigment epithelium or increased reflectivity in the choroid may also be capable of identifying localized RPE atrophy. Lujan et al.[23] took advantage of this phenomenon and described the possibilities of OCT fundus imaging to outline GA in a small patient series. Even though this approach is comparatively easy to perform, it may be confounded by numerous phenomena because it relies on the sum of OCT images. Hence, the additional depth information provided by PS-SD-OCT is lost. Additional studies are clearly warranted to investigate its suitability for daily use, especially in patients with media opacities and different degrees of RPE pigmentation.

In this study, we introduced PS-SD-OCT as a useful tool for identifying characteristic patterns of FSL in different stages of AMD. We chose to superimpose our segmentation results onto reflectivity based B-scan images to directly compare and check the performance of the segmentation algorithm with the true morphologic situation. Data showed that FSLs within the retinal pigment epithelium are increasingly present with disease severity in advanced stages of AMD, indicating the clinical importance of PS-SD-OCT technology because FSLs cannot be detected in fundus photography or angiography. Notably, discrete FSL lesions could be detected in some patients with drusen, whereas large areas of depolarization loss corresponded to the atrophic zones identified in GA and fibrotic scars.

Ten of 11 patients with nAMD had significant FSLs in addition to morphologic RPE irregularities, indicating that substantial RPE loss might be one reason for the often limited functional outcome in these patients, even if appropriate and effective antiexudative therapy is applied with antiangiogenic agents. This is of particular interest for patients undergoing frequent anti-VEGF treatment in nAMD because FSLs are likely to be an important reason for persistently decreased visual acuity, which is frequently observed even though the retinal anatomy is restored after consequent antiangiogenic treatment. Moreover, data indicate that assessing treatment effects with retinal thickness analysis for study purposes may give only one piece of necessary information, whereas the status of the retinal pigment epithelium, with its potentially relevant role for central visual function, remains widely neglected. It is important to realize that FSLs cannot be detected with current SD-OCT because these systems do not allow for true tissue differentiation on the RPE level.

Limitations of this study are the small patient numbers and its cross-sectional design. Nevertheless, the authors believe that this patient population is adequate to demonstrate the ability of PS-SD-OCT to identify and automatically segment the retinal pigment epithelium in different stages of AMD, in contrast to the inability of current SD-OCT devices to visualize the retinal pigment epithelium properly. Prospective studies investigating the degree of RPE impairment and their correlation to central visual function are clearly essential and under way. Another limitation is that we did not perform autofluorescence measurements in all patients included in this study. This must be performed in future prospective trials, especially in GA, to determine how defects in the autofluorescence pattern correlate to RPE depolarization loss in PS-SD-OCT.

In conclusion, this study shows that RPE depolarization loss and FSLs are frequent findings in all advanced stages of AMD pointing to the drawbacks of current SD-OCT technology,

which is incapable of imaging this information of the real RPE damage appropriately. Although modern segmentation algorithms offered by SD-OCT systems of different manufacturers show generally good performance when applied to SD-OCT data sets, they fail to identify zones of FSL because information reflecting the functional status of the retinal pigment epithelium is absent in the data sets. On the contrary, PS-SD-OCT was able to detect atrophic zones within the retinal pigment epithelium reliably in this study, in accordance with previous reports. This unique ability of PS-SD-OCT opens the doors for true tissue differentiation and exact detection of atrophic areas in high-detail retinal imaging of macular disease. PS-SD-OCT is a powerful tool when combined with adequate segmentation analysis and 3D imaging modalities and enables assessment of both the retinal and the pigment epithelial status of patients with AMD.

Further studies are clearly needed to clarify the reasons for RPE atrophy and factors that influence it. There is certainly a need for studies showing the histologic basis for these new findings and correlating them to PS-SD-OCT in the same specimen. Moreover, correlations between other imaging modalities, such as fundus autofluorescence and PS-SD-OCT, are needed to allow for adequate classification and comparison of findings, especially in nonneovascular forms of AMD.

Acknowledgments

The authors thank Stefan Sacu, Ramzi Sayegh, and Michael Georgopoulos for patient recruitment, and Geraldine Stock for proofreading of the manuscript. High-definition OCT systems were provided by Carl Zeiss Meditec, California, and Heidelberg Engineering. PS-SD-OCT was constructed and provided by the Center for Biomedical Engineering and Physics, Medical University of Vienna, Austria.

Supported by the Austrian Science Fund (FWF Grant P19624-B02) and the European Commission FUN OCT (FP7 HEALTH, contract no. 201880).

References

1. Bressler NM, Bressler SB, Fine SL. Age-related macular degeneration. Surv Ophthalmol. 1988; 32(6):375–413. [PubMed: 2457955]
2. Coleman AL, Yu F. Eye-related Medicare costs for patients with age-related macular degeneration from 1995 to 1999. Ophthalmology. 2008; 115(1):18–25. [PubMed: 17572499]
3. Friedman DS, O'Colmain BJ, Munoz B, et al. Prevalence of age-related macular degeneration in the United States. Arch Ophthalmol. 2004; 122(4):564–572. [PubMed: 15078675]
4. Klein R, Klein BE, Linton KL. Prevalence of age-related maculopathy: the Beaver Dam Eye Study. Ophthalmology. 1992; 99(6):933–943. [PubMed: 1630784]
5. Vingerling JR, Dielemans I, Hofman A, et al. The prevalence of age-related maculopathy in the Rotterdam Study. Ophthalmology. 1995; 102(2):205–210. [PubMed: 7862408]
6. Ferrara N, Gerber HP, LeCouter J. The biology of VEGF and its receptors. Nat Med. 2003; 9(6): 669–776. [PubMed: 12778165]
7. Rosenfeld PJ, Brown DM, Heier JS, et al. Ranibizumab for neovascular age-related macular degeneration. N Engl J Med. 2006; 355(14):1419–1431. [PubMed: 17021318]
8. Bartlett H, Eperjesi F. Age-related macular degeneration and nutritional supplementation: a review of randomised controlled trials. Ophthalmic Physiol Opt. 2003; 23(5):383–399. [PubMed: 12950886]
9. Jaffe GJ, Caprioli J. Optical coherence tomography to detect and manage retinal disease and glaucoma. Am J Ophthalmol. 2004; 137(1):156–169. [PubMed: 14700659]
10. Srinivasan VJ, Wojtkowski M, Witkin AJ, et al. High-definition and 3-dimensional imaging of macular pathologies with high-speed ultrahigh-resolution optical coherence tomography. Ophthalmology. 2006; 113(11):2054 e1–e14. [PubMed: 17074565]

11. Schmidt-Erfurth U, Leitgeb RA, Michels S, et al. Three-dimensional ultrahigh-resolution optical coherence tomography of macular diseases. Invest Ophthalmol Vis Sci. 2005; 46(9):3393–3402. [PubMed: 16123444]
12. Fleckenstein M, Charbel Issa P, Helb HM, et al. High-resolution spectral domain-OCT imaging in geographic atrophy associated with age-related macular degeneration. Invest Ophthalmol Vis Sci. 2008; 49:4137–4144. [PubMed: 18487363]
13. Bolz M, Ritter M, Polak K, et al. The role of Stratus OCT in anti-VEGF therapy: qualitative and quantitative assessment of neovascular AMD. Ophthalmologe. 2008; 105(7):650–655. [PubMed: 18273622]
14. Sadda SR, Wu Z, Walsh AC, et al. Errors in retinal thickness measurements obtained by optical coherence tomography. Ophthalmology. 2006; 113(2):285–293. [PubMed: 16406542]
15. Ahlers C, Golbaz I, Stock G, et al. Time course of morphologic effects on different retinal compartments after ranibizumab therapy in age-related macular degeneration. Ophthalmology. 2008; 115(8):e39–e46. [PubMed: 18675694]
16. Pircher M, Götzinger E, Leitgeb R, et al. Imaging of polarization properties of human retina in vivo with phase resolved transversal PS-OCT. Opt Expr. 2004; 12(24):5940–5951.
17. Pircher M, Götzinger E, Findl O, et al. Human macula investigated in vivo with polarization-sensitive optical coherence tomography. Invest Ophthalmol Vis Sci. 2006; 47(12):5487–5494. [PubMed: 17122140]
18. Götzinger E, Pircher M, Hitzenberger CK. High speed spectral domain polarization sensitive optical coherence tomography of the human retina. Opt Expr. 2005; 13(25):10217–10229.
19. Götzinger E, Pircher M, Geitzenauer W, et al. Retinal pigment epithelium segmentation by polarization sensitive optical coherence tomography. Opt Expr. 2008; 16(21):16416–16428.
20. Michels S, Pircher M, Geitzenauer W, et al. Value of polarisation-sensitive optical coherence tomography in diseases affecting the retinal pigment epithelium. Br J Ophthalmol. 2008; 92(2): 204–209. [PubMed: 18227201]
21. Miura M, Yamanari M, Iwasaki T, et al. Imaging polarimetry in age-related macular degeneration. Invest Ophthalmol Vis Sci. 2008; 49(6):2661–2667. [PubMed: 18515594]
22. Ahlers C, Simader C, Geitzenauer W, et al. Automatic segmentation in three-dimensional analysis of fibrovascular pigment epithelial detachment using high-definition optical coherence tomography. Br J Ophthalmol. 2008; 92(2):197–203. [PubMed: 17965102]
23. Lujan B, Rosenfeld J, Gregori G, et al. Spectral domain optical coherence tomographic imaging of geographic atrophy. Ophthalmic Surg Lasers Imaging. 2009; 40:96–101. [PubMed: 19320296]

Europe PMC Funders Author Manuscripts

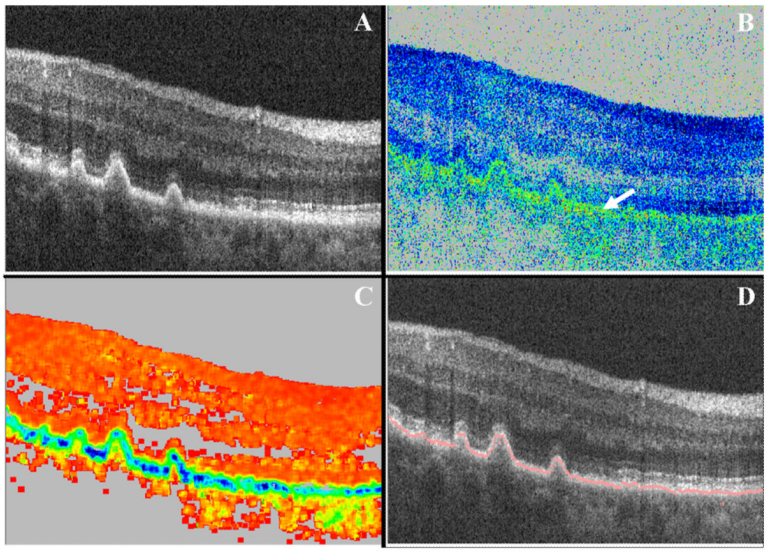

Figure 1.

This figure show how the following notations were generated in a patient with drusen and used to visualize intensity-based information in combination with polarization-scrambling properties of the RPE. The “intensity” image (**A**) shows the typical elevations of the retinal pigment epithelium well known from standard OCT technology, whereas the “retardation” image (**B**) shows a *greenish* band that is caused by the random retardation values from speckle to speckle. This information can clearly be associated with the retinal pigment epithelium (the color scale contains values between *blue* [0° retardation] and *red* [90° retardation]). The calculated DOPU image (**C**) shows an even better contrast of the retinal pigment epithelium in comparison with other structures of the retina (*red*, DOPU = 1; *black*, DOPU = 0). A composite image can be generated (**D**) showing the segmented retinal pigment epithelium (*red line*) projected on a normal intensity image. This approach demonstrates the performance of the automated segmentation algorithm using the DOPU information in comparison with the RPE appearance in the intensity image.

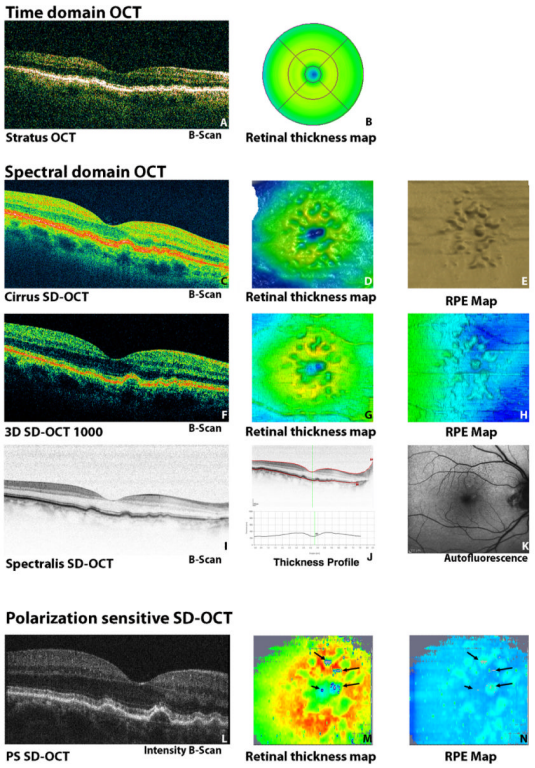

Figure 2.

Comparison of different OCT devices in drusen. Current SD-OCT instruments (**C–K**) are clearly superior to conventional time-domain OCT (**A**, **B**). Although the segmentation algorithms provided by OCT systems detect elevations of the retinal pigment epithelium correctly (**E**, **H**), they fail to detect FSLs of the retinal pigment epithelium, suggesting a continuous RPE pattern in this patient. The Spectralis OCT shows brilliant B-scan quality (**I**) but fails to segment the retinal pigment epithelium reliably (**J**). The autofluorescence image does not show a significant defect of the retinal pigment epithelium (**K**). PS-SD-OCT identifies the retinal pigment epithelium precisely (**L**) and visualizes small FSLs in the retinal pigment epithelium in the retinal thickness map (**M**) and in the RPE map (**N**). FSLs are indicated by arrows in (**N**) and are displayed in *gray* in the PS-SD-OCT–derived retinal thickness (**M**) and RPE elevation (**N**) maps.

Europe PMC Funders Author Manuscripts

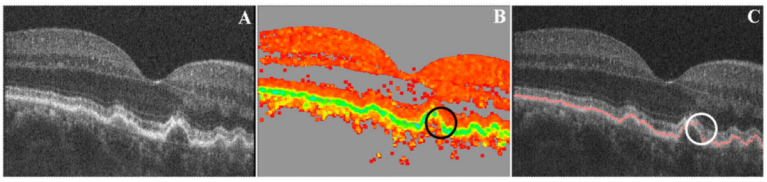

Figure 3.

Representative B-scan (same eye as in Fig. 2) with drusen showing a small FSL within the retinal pigment epithelium. Although the retinal pigment epithelium appears as a continuous layer in the intensity channel of a PS-SD-OCT data set (**A**), the DOPU image (**B**) clearly visualizes a small FSL (*circle*). The composite image (**C**) demonstrates the performance of the automated segmentation algorithm. Two of 11 patients with drusen had discrete FSL.

Europe PMC Funders Author Manuscripts

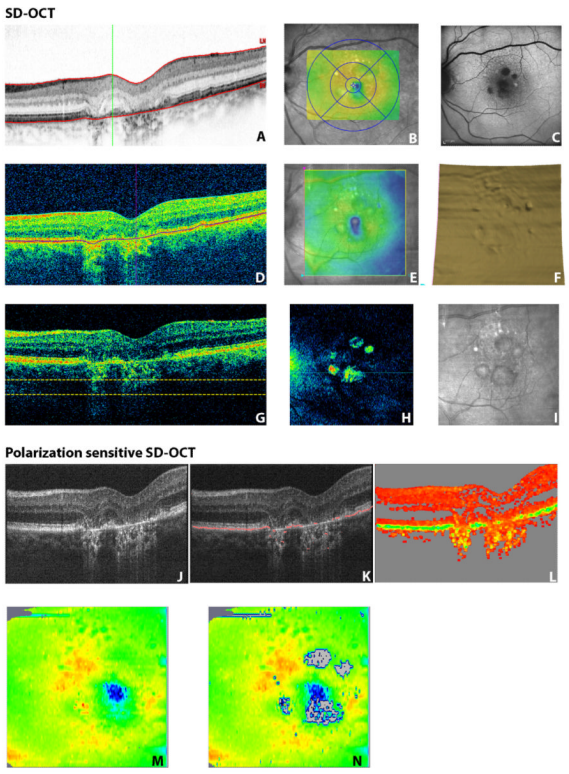

Figure 4.

Comparative imaging was performed in a patient with GA (**A**, **D**, **G**, **J**). Performance of the automatic segmentation in current SD-OCT devices (**A**, Spectralis; **D**, **G**, Cirrus) did not delineate RPE atrophy. RPE maps derived from conventional SD-OCT data failed to identify the atrophic zones (**F**), which clearly conflicts with the autofluorescence image (**C**). Like SD–OCT, PS-SD-OCT is able to visualize the well-known morphologic features of the atrophic zone in the intensity image (**J**), whereas the DOPU image correctly identifies residual RPE tissue and bridges of surviving retinal pigment epithelium (**L**) between the atrophic lesions. The composite image (**K**) shows the excellent performance of the automated segmentation algorithm. To allow a comparison with the commercially available instruments (**B**, **E**), (**M**) shows a “conventional” PS-SD-OCT thickness map defined as distance between ILM and outer retinal border. A different form of retinal thickness maps generated from PS-SD-OCT data (**N**) is capable of visualizing atrophic zones (shown in *gray*) in a retinal thickness map. Please note the correspondence of this map (**N**) to the SLO (**I**) and the autofluorescence image (**C**). Intensity-based “summation maps” (**H**) derived from summing up reflectivity data (**G**) are not able to delineate the contour of the RPE reliably in this patient.

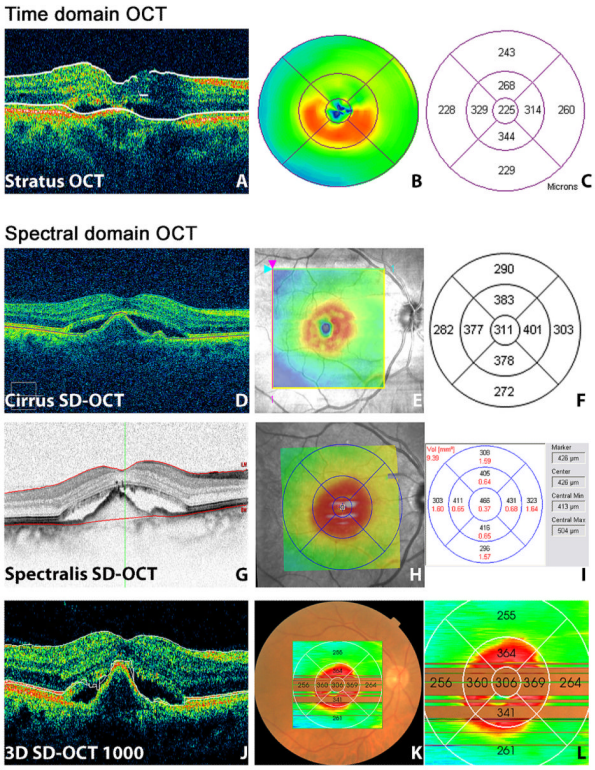

Figure 5.

Typical appearance of neovascular AMD in time-domain OCT (**A–C**) and SD-OCT (**D–F**, Cirrus; **G–I**, Spectralis; **J–L**, 3D-OCT 1000). Significant differences can be found in the retinal thickness reports (**C**, **F**, **I**, **L**). These differences are often caused by segmentation errors that can be observed in representative OCT B-scans (**A**, **D**, **G**, **J**).

Europe PMC Funders Author Manuscripts

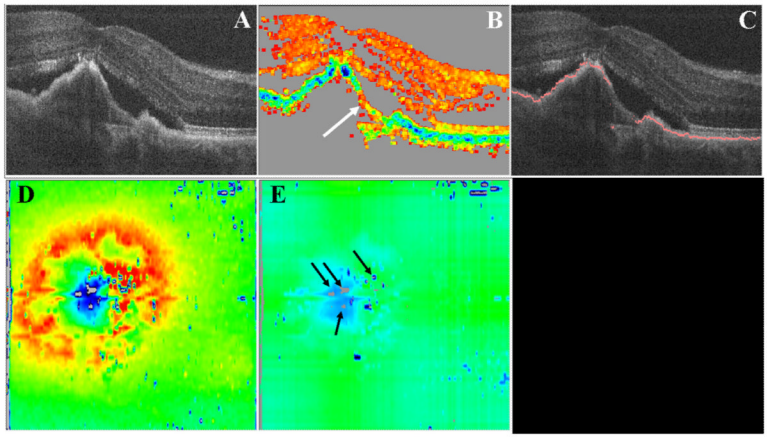

Figure 6.

PS-OCT in nAMD (same eye as in Fig. 5). The intensity image (**A**) corresponds well to conventional OCT (Fig. 5). However, the DOPU image (**B**) clearly identifies the retinal pigment epithelium and shows circumscribed focal atrophies (*white arrow*) and an irregular RPE pattern. The automatic RPE segmentation algorithm follows the outline of the retinal pigment epithelium (composite image, **C**). The retinal thickness map shows multiple focal RPE lesions in this treatment-naive patient (**D**, **E**) in close relation to the PED. Zones of RPE atrophy are displayed as *gray pixels* in these two maps.

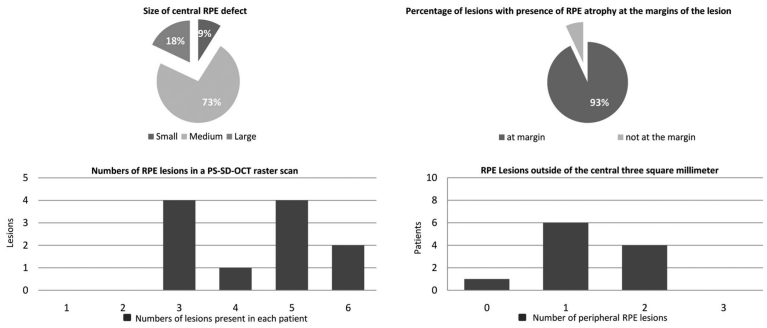

Figure 7.

Characteristics of pigment epithelial lesions in nAMD. Analysis shows that 10 of 11 patients with treatment-naive nAMD had significant FSLs within the retinal pigment epithelium within the 10 central B-scans obtained by PS-SD-OCT. Seventy-three percent showed medium RPE defects (diameter, 0.2– 0.5 mm), and 18% showed large RPE defects (diameter, >0.5 mm). Most patients showed FSLs at the margins of the lesion and presented with multiple FSLs. Small peripheral RPE lesions (located outside the central 3 mm) were also present in most patients with nAMD.

Europe PMC Funders Author Manuscripts

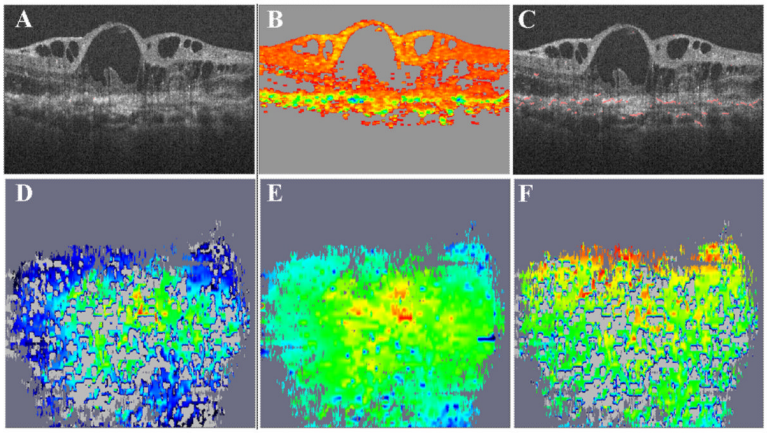

Figure 8.

Chorioretinal scar caused by nAMD. Residual retinal pigment epithelium cannot be differentiated from scarred structures because both appear as hyperreflective tissues in intensity-based OCT B-scans (**A**). PS-OCT reveals residual depolarizing tissue within the hyperreflective scar tissue complex and an irregular pattern of focal agglomerations of depolarizing structures within the scarred area that can be observed in the DOPU and the composite images (**B**, **C**). Retinal thickness maps (**D**, with RPE lesions in *gray*; **E**, with continuous retinal pigment epithelium and slightly differing color scale) demonstrate scattered areas of RPE atrophy (in *light g*ray; areas with low signal intensity are displayed in *dark gray*). The RPE elevation map (**F**) reveals both RPE atrophy and focal RPE elevations.